Spin quantum jumps in a singly charged quantum dot

M. P. van Exter, J. Gudat, G. Nienhuis, and D. Bouwmeester
Huygens Laboratory, Leiden University, P.O. Box 9504, 2300 RA Leiden, The Netherlands
(Received 27 March 2009; published 18 August 2009)

We model the population and coherence dynamics of a singly charged quantum dot driven by a constant optical field. Using a separation of time scales we predict the occurrence of quantum jumps in the spin state of the excess electron or hole. Our analysis extends the description of intermittent fluorescence from a three-level to a four-level description; the former is common in atomic systems, the later occurs in many solid-state systems. The statistics of the quantum jumps as function of the intensity of the driving field provide detailed information on physical processes that limit the ground-state coherence of these systems and their use as a solid-state quantum bit. In particular it enables a discrimination of coherent spin coupling, induced by the nuclear magnetic field, from incoherent spin flips; the coherent coupling can gradually be suppressed by increasing the pump intensity due to the quantum Zeno effect.

DOI: 10.1103/PhysRevA.80.023812 PACS number(s): 42.50.Lc, 73.21.La

I. INTRODUCTION

The spin of a single charge confined to an optically active quantum dot can be considered as a solid-state quantum bit [1–3]. It is an attractive candidate because most spin relaxation is quenched in quantum dots [4] and the coherence between its two ground states is long lived; lifetimes in excess of 1 μs are expected [5], relative to the sub 1 ns time scale for optical interactions with the spin. The spin state is optically addressed by addition of an exciton, resulting in the transfer to a short-lived charged exciton (=trion) state [6,7]. Optical readout can be efficient by embedding the quantum dot in a high-finesse microcavity [8–13]. It has been shown that a single quantum dot can change the cavity reflectivity from 0 to 50% [7], while theory predicts that this value can even reach 100% for realistic devices [14]. Alternative optical readout techniques, which are based on the Faraday or Kerr effect and thus intrinsically spin selective, are generally less efficient [15,16].

Based on the analysis presented in this paper, we predict the occurrence of sudden jumps between well defined, approximately stationary, spin states of the quantum dot. This prediction is a generalization of the quantum jumps that are known to occur in three-level systems. The latter jumps were originally proposed by Dehmelt [17], who described them in terms of "electron shelving" from a strong optical (cycling) transition to a weakly interacting level and explained how the statistics of the intermittent fluorescence can be used to analyze weak transitions in single-atom spectroscopy. Cook and Kimble [18] predicted that under continuous incoherent excitation the observed fluorescence should randomly switch "on" and "off," giving a random telegraph signal. The first experiments on trapped atoms were performed in the 1980's by Wineland *et al.* [19], Bergquist *et al.* [20], and Kimble *et al.* [21]. Blinking statistics in single semiconductor nanocrystal quantum dots have been observed by Shimizu [22]. An excellent review of the theoretical aspects of the quantum jump approach has been written by Plenio and Knight [23].

In this article we will analyze the optically driven dynamics of a singly charged self-assembled quantum dot modeled as a four-level system. Such systems can potentially exhibit a wide range of intriguing dynamical processes, such as coherent population trapping, electromagnetically induced transparency, and lasing without inversion (see, e.g., ref [24] and references therein). In our quantum dot system, most quantum-interference effects are effectively removed by the relatively fast spontaneous decay from the two upper levels to the two lower levels. This fast decay allows for a separation of time scales between the various dynamical processes and a description in terms of effective populations and jump rates.

The optical transition in quantum dots differs in a crucial way from that in free atoms. The quantum dot has a natural quantization axis, set by its growth direction and pancake shape, whereas the free atom is rotationally symmetric. The resulting energy separation between the heavy-hole ($m=\pm\frac{3}{2}$) and light-hole ($m=\pm\frac{1}{2}$) states allows one to experimentally single out the optical transition to the heavy-hole exciton states, thus creating a natural preference for the spin basis. The spontaneous emission from this transition aimed dominantly toward the quantization axis and is circularly polarized in this direction. Other processes that are included in the model are coherent coupling between the electron or hole spin levels due to interaction with the nuclei of the semiconductor host material [25], spontaneous spin flips due to interaction with the phonon bath, and coherent coupling between ground and excited states due to the driving optical field [26]. The field-induced coupling is assumed to be constant and described by two fixed Rabi frequencies Ω_+ and Ω_- for the right-handed and left-handed circularly polarized light. This relatively simple and clean case with constant coupling rate will be analyzed in detail. The outline of a refined model that includes the back action of the electron spin on the nuclear spin and the intracavity field will be given in Sec. V.

The paper is organized as follows. Section II introduces the key parameters that describe the dynamics of a general four-level system. Section III discusses the separation of time scales, both from a general point of view and applied to our four-level system, and provides a relatively simple expression for the quantum jump rates due to incoherent spin flips. Section IV deals with the more intriguing quantum

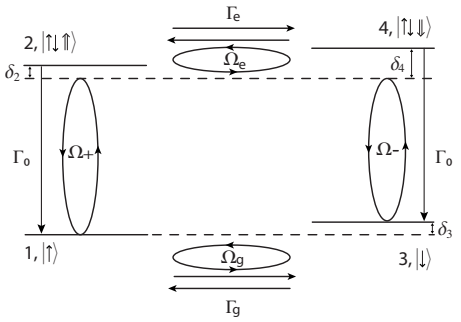

FIG. 1. Energy levels and internal dynamics in our four-level system comprising two ground-state levels (1 and 3) of a single electron in a quantum dot and the two excited singly charged exciton (=trion) levels X^- (2 and 4). Possible frequency detunings are indicated as δ_2, δ_3, and δ_4. The two "spin-up" levels (1 and 2) on the left-hand size are coupled by right-handed circularly polarized light; the two "spin-down" levels (3 and 4) require light with a left-handed polarization. Spontaneous decay from the trion levels to the ground states occurs at a rate Γ_0. Different spin states are coupled by coherent and incoherent processes. The coherent coupling frequencies are denoted by Ω_g and Ω_e for the two ground-state and excited-state levels, respectively. The incoherent spin flip process is assumed to be symmetric and denoted by population decay rates Γ_g and Γ_e. A similar level scheme is applicable to positively charged quantum dots and many other symmetric four-level systems.

jumps due to coherent spin coupling. Section V discussed the experimental possibilities and the outline of a refined model. Section VI contains the concluding discussion.

II. INTRODUCING THE FOUR-LEVEL SYSTEM

Figure 1 shows the energy levels in the proposed four-level model of the singly charged quantum dot and the relevant coupling and decay rates. We choose to describe the dynamics of a negatively charged quantum dot, but the results apply equally well to positively charged devices. The two lower or ground-state levels (1 and 3) contain a single electron pointing either up $|\uparrow\rangle$ or down $|\downarrow\rangle$. The two upper or excited-state levels (2 and 4) are the two charged exciton (=trion) states, comprising an electron pair (spin neutrality imposed by the Pauli principle) and an additional heavy hole; these levels are denoted as $|\uparrow\downarrow\Uparrow\rangle$ and $|\uparrow\downarrow\Downarrow\rangle$. A possible frequency splitting between the two ground states, caused by the "out-of-plane" component of the (nuclear) magnetic field, i.e., the component parallel to the growth direction, is denoted as $\delta_3 \equiv \omega_{31} \equiv \omega_3 - \omega_1$. This nuclear magnetic field varies slowly on a typical time scale of micro to milliseconds, depending on temperature, external field and material composition [27]. In our model we will treat it as a quasistatic field, i.e., as if the fluctuations are frozen in time [28]. Fluctuations that do occur and are integrated over experimentally will show up as an additional decoherence, being the "pure dephasing" or T_2^* component of the total decoherence time T_2 [27]. The two other frequency splittings are defined with respect to the optical frequency ω_0 of the optical pump as $\delta_2 \equiv \omega_{21} - \omega_0$ and $\delta_4 \equiv \omega_{41} - \omega_0$. These splittings depend on the circular anisotropy; linear anisotropies, due to mechanical strain and crystal-field effects, are described by a coherent coupling between the spin levels. The exciton fine structure splitting observed in neutral quantum dots with asymmetric shapes [29] is absent in singly charged quantum dots [30]. The populations and coherences in the four-level system are contained in a 4×4 density matrix $\rho(t)$. The evolution of this matrix is described in a rotating basis with the two upper states rotating at a frequency ω_0 with respect to the two ground states. Before doing so, we will present the relevant interactions, which we separate in four coupling channels and six decay channels. A crucial aspect of our analysis will be the distinction between "spin-conserving transitions," which occur either from levels $1 \leftrightarrow 2$ or $3 \leftrightarrow 4$, and "spin-changing transitions," which occur either from levels $1 \leftrightarrow 3$ or $2 \leftrightarrow 4$.

We distinguish four coherent interactions, indicated by closed loops in Fig. 1. The optical field creates a coherent coupling between ground and excited states of equal handedness. Optical excitation with right handed circularly polarized light results in a coherent coupling of the spin-up states (1 and 2) at a frequency $\Omega_{1\leftrightarrow 2} \equiv \Omega_+$; excitation with left handed circularly polarized light results in a coherent coupling of the spin-down state (3 and 4) at a frequency $\Omega_{3\leftrightarrow 4} \equiv \Omega_-$. A possible "in-plane" (nuclear) magnetic field, or any other linear anisotropy, will induce a coherent coupling between spin states of opposite handedness. The two ground states are connected via a coherent coupling frequency $\Omega_{1\leftrightarrow 3} \equiv \Omega_g$; the two excited states are connected via a coupling frequency $\Omega_{2\leftrightarrow 4} \equiv \Omega_e$. These rates can differ on account of the different g factors for electrons and holes. The evolution induced by the mentioned coherent coupling frequencies and frequency splittings can be summarized in a single Hamiltonian

$$H = -\frac{\hbar}{2}\begin{pmatrix} 0 & \Omega_+ & \Omega_g & 0 \\ \Omega_+ & 2\delta_2 & 0 & \Omega_e \\ \Omega_g & 0 & 2\delta_3 & \Omega_- \\ 0 & \Omega_e & \Omega_- & 2\delta_4 \end{pmatrix}. \tag{1}$$

We distinguish six incoherent interactions, indicated by straight arrows in Fig. 1. Spontaneous emission of photons results in population decay from the two excited states (2 and 4) to the associated ground states (1 and 3) at rates $\Gamma_{2\to 1} = \Gamma_{4\to 3} \equiv \Gamma_0$; these decay rates can possibly be enhanced with respect to their free-space value by the Purcell effect [7]. The ground states (1 and 3) are connected via two complementary decay processes at rates $\Gamma_{1\to 3} = \Gamma_{3\to 1} \equiv \Gamma_g$; the two excited states are connected via similar rates $\Gamma_{2\to 4} = \Gamma_{4\to 2} \equiv \Gamma_e$. These incoherent spin flips are induced by interaction with the phonon bath. All six incoherent processes can be described by a jump evolution and are associated with quantum noise on account of the (quantum) fluctuation-dissipation theorem.

The full 4×4 density matrix evolves as

$$\frac{d}{dt}\rho = \mathcal{L}\rho, \tag{2}$$

where $\mathcal{L}$ is the Liouville superoperator. This superoperator naturally separates into one contribution from each coupling

or decay channel. Coherent coupling between two levels $i \leftrightarrow j$ leads to a Rabi oscillation between the populations ρ_{ii} and ρ_{jj} and coherence ρ_{ij} $(=\rho_{ji}^{*})$ of these levels. This evolution, which would be reversible if it was the only coupling process, is described by a superoperator of the form $\mathcal{L}_{\mathrm{coh},i\leftrightarrow j}\rho=(1/i\hbar)[H_{i\leftrightarrow j},\rho]$. Incoherent population decay from level j to i is an irreversible process associated with a coupling to a large reservoir (often denoted as the "bath"); it results in a one-way exponential decay that can be described by the Liouville superoperator $\mathcal{L}_{\mathrm{inc},j\rightarrow i}$. The two mentioned superoperators have the mathematical form

$$\mathcal{L}_{\mathrm{coh},i\leftrightarrow j}=i\frac{\Omega_{ij}}{2}(|j\rangle\langle i|\rho+|i\rangle\langle j|\rho-\rho|j\rangle\langle i|-\rho|i\rangle\langle j|), \tag{3}$$

$$\mathcal{L}_{\mathrm{inc},j\rightarrow i}=\frac{\Gamma_{j\rightarrow i}}{2}(2|i\rangle\langle j|\rho|j\rangle\langle i|-\rho|j\rangle\langle j|-|j\rangle\langle j|\rho), \tag{4}$$

where Ω_{ij} is a Rabi frequency and $\Gamma_{j\rightarrow i}$ is an incoherent population decay rate. The full superoperator $\mathcal{L}$ is a simple sum over ten terms associated with the four coupling channels and six decay channels that are selected. Although we find our choice a natural one, other authors might prefer to start from different level dynamics [31]. The analysis discussed below can be applied to any of these models.

III. SEPARATION OF TIME SCALES

A. General framework

The dynamics of the four-level system can be described by an approximate evolution equation, that is based on a separation of time scales, as discussed in ref [32]. The various terms in the superoperator $\mathcal{L}$ are separated in large and small terms, corresponding to rapid and slow evolution. The coupling between the spin-up states 1 and 2 and the coupling between the spin-down states 3 and 4 are generally strong compared to the coupling between the two ground states 1 and 3 and the coupling between the two excited states 2 and 4. In the scheme of Fig. 1, the vertical transitions are the strong ones, while the horizontal transitions are weak. Moreover, the Rabi frequencies Ω_e and Ω_g are linear in the coupling matrix elements, whereas the rates Γ_e and Γ_g are quadratic in these couplings (this is part of Fermi's golden rule). Therefore, it is consistent to treat Ω_e and Ω_g as first-order terms in a smallness parameter, and Γ_e and Γ_g as second order. This implies that we separate the Liouville operator as $\mathcal{L}=\mathcal{L}_0+\mathcal{L}_1+\mathcal{L}_2$. The zeroth-order operator term $\mathcal{L}_0$ contains the matrix elements δ_i, Γ_0 and $\Omega_{\pm}$, while the Rabi frequencies Ω_g and Ω_e contribute to the first-order operator $\mathcal{L}_1$. The second-order operator $\mathcal{L}_2$ contains the remaining matrix elements Γ_g and Γ_e.

The basis idea of the separation of time scales is that on the rapid time scale, $\mathcal{L}_0$ drives the system to a quasisteady state. This happens before the slow terms, described by $\mathcal{L}_1$ and $\mathcal{L}_2$, have had time to cause any change. Since in the present case the operator $\mathcal{L}_0$ does not couple the spin-up states (1 and 2) to the spin-down states (3 and 4), or vice versa, the parameters determining the quasisteady state are the population $n_+(t)$ of the spin-up states and $n_-(t)$ of the spin-down states. On the long time scale, the operators $\mathcal{L}_1$ and $\mathcal{L}_2$ mix the spin-up states and the spin-down states, so that the populations n_+ and n_- can change. This causes a slow evolution of the system through the subspace of steady states with respect to $\mathcal{L}_0$.

The equation for the slow evolution is obtained when we present the operator $\mathcal{P}$ that projects any density matrix on the space of the quasisteady states. This space is the eigenspace of $\mathcal{L}_0$ with eigenvalue zero. This implies that $\mathcal{L}_0$ gives zero when acting on the projected part $\mathcal{P}\rho$ for any density matrix, making $\mathcal{L}_0\mathcal{P}=0$. Moreover, the rapid evolution can only cause changes within this eigenspace, so that also $\mathcal{P}\mathcal{L}_0=0$. As a result, the evolution of $\mathcal{P}\rho$ occurs exclusively on the slow time scale, determined by $\mathcal{L}_1$ and $\mathcal{L}_2$. The complementary projection operator is $\mathcal{Q}=1-\mathcal{P}$, and both operators obey the defining property of a projection operator $\mathcal{P}^2=\mathcal{P}$, $\mathcal{Q}^2=\mathcal{Q}$. The Liouville Eq. (2) can be separated into the exact equations

$$\frac{d}{dt}\mathcal{P}\rho=\mathcal{P}(\mathcal{L}_1+\mathcal{L}_2)\mathcal{P}\rho+\mathcal{P}(\mathcal{L}_1+\mathcal{L}_2)\mathcal{Q}\rho, \tag{5}$$

$$\frac{d}{dt}\mathcal{Q}\rho=\mathcal{Q}(\mathcal{L}_1+\mathcal{L}_2)\mathcal{P}\rho+\mathcal{Q}\mathcal{L}\mathcal{Q}\rho. \tag{6}$$

In order to arrive at an equation for $\mathcal{P}\rho$ alone, we eliminate $\mathcal{Q}\rho$ by formally solving Eq. (6) and substituting the result in Eq. (5). By restricting the result to second order, this gives the result

$$\frac{d}{dt}\mathcal{P}\rho=\mathcal{P}(\mathcal{L}_1+\mathcal{L}_2)\mathcal{P}\rho+\mathcal{P}\mathcal{L}_1\int_0^{\infty}d\tau\exp(\mathcal{L}_0\tau)\mathcal{Q}\mathcal{L}_1\mathcal{P}\rho(t). \tag{7}$$

In the present system, this expression can be used to calculate the slow spin dynamics.

B. Application to our four-level system

The described separation of time scales is an ideal tool to simplify the dynamics of the four-level system depicted in Fig. 1, as it allows to separate the dominant (fast) evolution from the weaker (and slower) components. For this separation we assume all spin-changing rates to be relatively small in comparison with the spontaneous lifetime of the excited state, i.e., $\{\Gamma_g,\Gamma_e,\Omega_g,\Omega_e\}\ll\Gamma_0$. On top of that we distinguish the weak-pumping limit ($\{\Omega_-,\Omega_+\}\ll\Gamma_0$) from the regime of moderate to strong optical excitation. In the weak-pumping limit the two upper levels are barely excited and the level dynamics is dominated by the interaction between the two ground states; this limit is discussed briefly in Sec. IV C. Most of our discussion, however, will focus on the regime of moderate to strong optical excitation.

For moderate to strong optical fields, the cycling dynamics in the two optical transitions will quickly exceed any spin transition rate. This regime enables the separation of time scales discussed in Sec. III A, where the fast dynamics associated with the optical transitions is combined in the operator

$\mathcal{L}_0$. As the optical transitions are spin conserving, the total spin-up population $n_+=\rho_{11}+\rho_{22}$ and the total spin-down population $n_-=\rho_{33}+\rho_{44}$ are both invariant under operation of $\mathcal{L}_0$. The projection operator $\mathcal{P}$ associated with $\mathcal{L}_0$ thus projects the density matrix in the two spin subspaces, making

$$\mathcal{P}\rho(t) = n_+(t)\bar{\rho}_+ + n_-(t)\bar{\rho}_-. \tag{8}$$

The submatrices

$$\bar{\rho}_\pm = \begin{pmatrix} (1-\alpha_\pm) & c_\pm \\ c_\pm^* & \alpha_\pm \end{pmatrix}, \tag{9}$$

describe the steady-state distributions within the two optical transitions, where

$$\alpha_\pm = \frac{\Omega_\pm^2}{\Gamma_0^2 + 2\Omega_\pm^2 + (2\delta_\pm)^2}, \tag{10}$$

$$c_\pm = \frac{-2\delta_\pm - i\Gamma_0}{\Gamma_0^2 + 2\Omega_\pm^2 + (2\delta_\pm)^2}, \tag{11}$$

are the excited-state fraction and (complex) coherence, respectively. The frequency detunings are $\delta_+=\delta_2$ and $\delta_- \equiv \delta_4 - \delta_3$, respectively.

We solve for the dynamics of the spin populations $n_+(t)$ and $n_-(t)$ by substituting the $\mathcal{P}$ projection specified by Eqs. (8) and (9) in the general Eq. (7). This substitution results in a generic expression of the form

$$\frac{d}{dt}n_+(t) = -R_{+\to-}n_+(t) + R_{-\to+}n_-(t) = -\frac{d}{dt}n_-(t). \tag{12}$$

Explicit expressions for the jump rates $R_{+\to-}$ from the spin up to the spin-down manifold and the jump rate $R_{-\to+}$ for the reverse process can be calculated through substitution of $\mathcal{L}_0$, $\mathcal{L}_1$, and $\mathcal{L}_2$ in the appropriate expressions. This is the most difficult part of the calculation; it will be discussed in the next subsections.

Equation (12) can be interpreted in terms of two population operators with eigenvalues $n_\pm=\{0,1\}$ and quantum jumps between two spin manifold. The jumps occur naturally and are driven by the internal population dynamics and quantum noise. Alternatively, one could stress the importance of quantum state projection through observation [23]. In this description, the optical cycling transitions within each manifold creates quantum entanglement between the atomic spin state and the handedness of the optical emission, thus allowing one to extract information on the spin state by (projective) measurements on the optical field. This situation is similar to that found in intermittent fluorescence, where the optical measurement enables one to decide whether the atomic population is located in the optically active manifold or in the dark "shelving" state [17,21].

C. Two contributions to the jump rates

Essential ingredients in our analysis is the separation of the 4×4 density matrix ρ into four blocks of 2×2 elements that combine kets and bras with the same spin combinations, making the action of the superoperators $\mathcal{L}_1$ and $\mathcal{L}_2$ on these blocks quite different. The operator $\mathcal{L}_1$, associated with coherent coupling at Rabi frequencies Ω_g and Ω_e, only transfers elements from the diagonal blocks to the off-diagonal blocks of ρ and vice versa. The operator $\mathcal{L}_2$, associated with incoherent spin flips at rates Γ_g and Γ_e, mixes elements within each block and only transfers elements between the diagonal blocks. As a result of this blocklike operation the term $\mathcal{P}\mathcal{L}_1\mathcal{P}\rho=0$ in Eq. (7). Furthermore, the quantum jump rates separate as $R=R_{\rm inc}+R_{\rm coh}$, where $R_{\rm inc}$ and $R_{\rm coh}$ are the "incoherent" and "coherent" contributions associated with $\mathcal{L}_2$ and $\mathcal{L}_1$, respectively. The incoherent contribution to the jump rates are easily calculated as

$$R_{{\rm inc},+\to-} = (1-\alpha_+)\Gamma_g + \alpha_+\Gamma_e, \tag{13}$$

$$R_{{\rm inc},-\to+} = (1-\alpha_-)\Gamma_g + \alpha_-\Gamma_e. \tag{14}$$

They are the averages of the spin flip rates between the ground and excited state, weighted over the relative excited-state populations $\alpha_\pm$. A calculation of the coherent contributions $R_{\rm coh}$ takes more effort and will be dealt with in the next section.

IV. JUMP RATE DUE TO COHERENT SPIN COUPLING

A. General remarks

A calculation of the jump rate induced by coherent spin coupling requires some serious bookkeeping, for which we use the computer program Mathematica. We again benefit from the blocklike operation of the superoperators, which allows to evaluate the complicated second term in Eq. (7) in three steps. Starting from the diagonal matrix $\mathcal{P}\rho$ on the right-hand site, (i) the operation $\mathcal{L}_1$ transfers coherence to the off-diagonal blocks, (ii) the integral operation modifies the off-diagonal elements, and (iii) the final operation $\mathcal{P}\mathcal{L}_1$ brings these elements back to the on-diagonal blocks where they contribute to the evolution of the spin populations n_+ and n_-. The most complicated part in this calculation is the integral operation in step (ii), which involves the inversion of the 4×4 matrix that describes the dynamics in the 2×2 off-diagonal block. Unfortunately, the resulting general expressions are quite lengthy and some results will thus be presented only in numerical form. To keep the equations short we will discuss the following special case: (i) a frequency-degenerate system ($\delta_2=\delta_3=\delta_4=0$) under various forms of excitation, (ii) the same system in the weak-pumping limit, and (iii) a detuned system with $\delta_3\neq0$ and $\delta_2, \delta_4 \ll \Gamma_0$.

B. Jump rate in a frequency-degenerate system

We will first consider a frequency-degenerate system ($\delta_2=\delta_3=\delta_4=0$). Applying the three-step procedure mentioned above, we find the following expression for the coherent jump rate from the two spin-up to the two spin-down levels

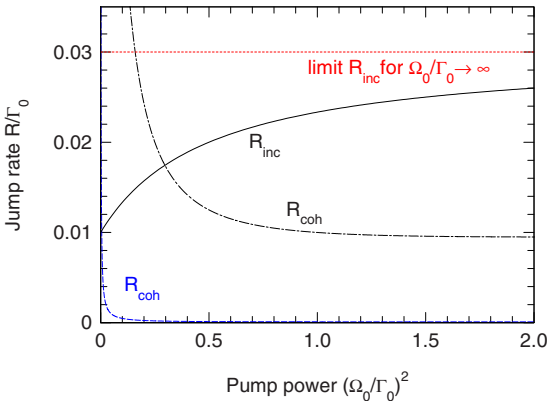

FIG. 2. (Color online) Calculated jump rates $R_{-\to+}=R_{+\to-}$ as function of the optical intensity of linearly polarized light, expressed as $\Omega_+^2=\Omega_-^2=\Omega_0^2$. The solid curve shows how the jump rate $R_{\rm inc}$ due to incoherent spin flips changes gradually from its "ground-state" value of Γ_g to an average value of $(\Gamma_g+\Gamma_e)/2$ for saturated excitation (parameters: $\Gamma_g=0.01$, $\Gamma_e=0.05$). The two dashed curves shows the jump rate due to coherent spin coupling for $\Omega_g=\Omega_e=0.01$ [dashed (blue) curve] and $\Omega_g=\Omega_e=0.1$ [dashed-dotted (black) curve]. All units are normalized to the spontaneous emission rate Γ_0. Note the pronounced decrease in $R_{\rm coh}$ at larger pump rates and the divergence for $\Omega_0\to 0$; this divergence can be removed by including other decay processes in the description (see Fig. 4).

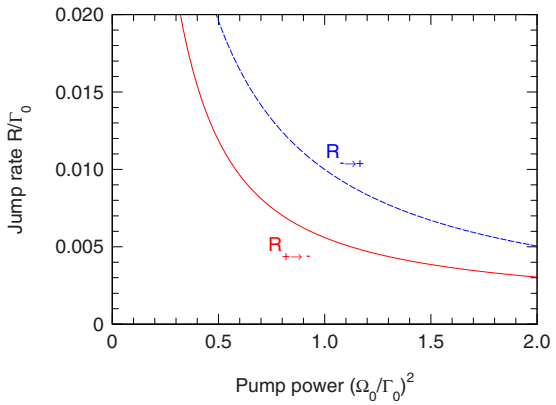

FIG. 3. (Color online) Demonstration of spin-selective jump rates $R_{\rm coh}$ for circularly polarized excitation. The jump rates due to coherent spin coupling are calculated as function of the intensity of right-handed circularly polarized light, expressed as Ω_+^2 ($\Omega_-=0$). The two curves show the jump rate $R_{{\rm coh},+\to-}$ from the spin up to the spin-down manifold [solid (red) curve] and the jump rate $R_{{\rm coh},-\to+}$ for the reverse jumps [dashed (blue) curve] for $\Omega_g=\Omega_e=0.1$, $\Gamma_g=\Gamma_e=0.01$, and $\delta_3=0$. All units are normalized to Γ_0. The resulting unbalance in spin population depends on the ratio of the two depicted jump rates $R_{\rm coh}$ and the jump rate $R_{\rm inc}$ associated with incoherent spin flips.

$$R_{{\rm coh},+\to-} = \frac{2\Gamma_0^5\Omega_g^2+\Gamma_0^3(\Omega_+^2+\Omega_-^2)\Omega_g^2+2\Gamma_0\Omega_+^2(\Omega_-\Omega_g+\Omega_+\Omega_e)^2}{(\Gamma_0^2+2\Omega_+^2)[2\Gamma_0^2(\Omega_+^2+\Omega_-^2)+(\Omega_+^2-\Omega_-^2)^2]}, \tag{15}$$

where we naturally assumed $\{\Gamma_g,\Gamma_e\}\ll\Gamma_0$. The jump rate $R_{{\rm coh},-\to+}$ for the reverse process is described by a similar expression that only differs in its spin labels, which are now swapped by the transformation $+\leftrightarrow-$.

Figure 2 shows three typical examples of the dependence of the jump rates on the optical intensity of linearly polarized light, expressed as $\Omega_+^2=\Omega_-^2=\Omega_0^2$. This figure highlights the pronounced difference between the power dependence of the jump rates due to the coherent and incoherent spin-changing processes. The solid curve shows how the "incoherent" jump rate $R_{\rm inc}$ changes gradually from its weak-pumping value of Γ_g to its strong pumping value $(\Gamma_g+\Gamma_e)/2$ on account of the increased excited-state populations. The dashed (blue) and dashed-dotted (black) curves show the power dependence of the "coherent" jump rate $R_{\rm coh}$ for two different values of the coherent coupling frequencies $\Omega_g=\Omega_e$. Under linearly polarized excitation the jump rate of Eq. (15) reduces to

$$R_{{\rm coh},+\to-}=R_{{\rm coh},-\to+}=\left(\frac{\Gamma_0}{2\Omega_0^2}\right)\left(\frac{(1+\beta)\Omega_g^2+\beta^2(\Omega_g+\Omega_e)^2}{(1+2\beta)}\right), \tag{16}$$

where $\beta\equiv(\Omega_0/\Gamma_0)^2\propto I/I_{\rm sat}$ measures the degree of saturation. This jump rate diverges in the weak-pumping limit and decreases to a limiting value $(\Omega_g+\Omega_e)^2/(2\Gamma_0)$ for strong pumping.

Figure 3 shows a typical example of the power dependence of the jump rates $R_{\rm coh}$ under excitation with right-handed circularly polarized light ($\Omega_-=0$). Optical excitation with circularly polarized light leads to an unbalance between the two jump rates

$$R_{{\rm coh},+\to-}=\frac{\Gamma_0}{1+2\Omega_+^2/\Gamma_0^2}\left[\frac{\Omega_g^2}{\Omega_+^2}+\frac{\Omega_+^2\Omega_e^2}{\Gamma_0^2(\Gamma_0^2+\Omega_+^2/2)}\right], \tag{17}$$

$$R_{{\rm coh},-\to+}=\frac{\Omega_g^2}{\Omega_+^2}\Gamma_0. \tag{18}$$

This unbalance is clearly visible in Fig. 4, which was calculated for an intrinsically "balanced" system with equal ground- and excited-state spin dynamics at $\Omega_g=\Omega_e=0.1\Gamma_0$ and $\Gamma_g=\Gamma_e=0.01\Gamma_0$. The difference between the two jump rates can be more pronounced in an "unbalanced" system. The mentioned difference will result in optical pumping from one spin manifold to the other and in an unbalance of the steady-state spin population ($\bar{n}_+\neq\bar{n}_-$), as determined by the balance $R_{+\to-}\bar{n}_+=R_{-\to+}\bar{n}_-$ with $R=R_{\rm coh}+R_{\rm inc}$.

C. Weak-pumping limit and the quantum Zeno effect

The weak-pumping limit ($\Omega_-,\Omega_+\ll\Gamma_0$) of Eq. (15) simplifies to

$$R_{{\rm coh},+\to-}\approx\left(\frac{\Omega_g^2}{\Omega_+^2+\Omega_-^2}\right)\Gamma_0, \tag{19}$$

if we also assume that $\Omega_e/\Omega_g\ll(\Omega_+/\Gamma_0)^2$. This jump rate diverges at zero pumping. The corresponding monotone decrease at increased pumping is a manifestation of the quantum Zeno effect [33]; it shows how repeated inspection of a

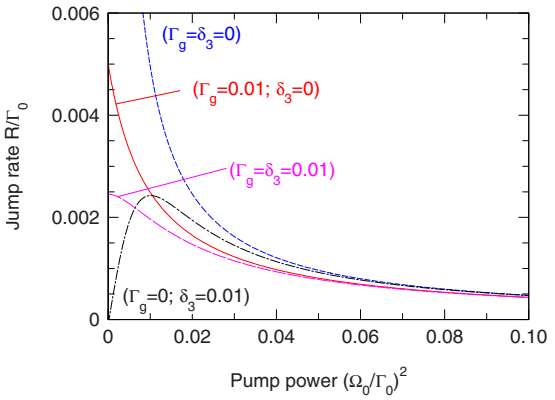

FIG. 4. (Color online) Calculated jump rates $R_{-\to+}=R_{+\to-}$ due to coherent spin coupling as function of the optical intensity of linearly polarized light, expressed as $\Omega_+^2=\Omega_-^2=\Omega_0^2$. The dashed (blue) curve is just a zoom in of a similar result depicted in Fig. 2 for $\Omega_g=\Omega_e=0.01$. The other three curves show how the divergence at low pump rate can be removed by inclusion of other decay processes in the description (see text). We have included only spin flips [solid (red) curve with $\Gamma_g=0.01$, $\delta_3=0$], only frequency detuning [dot-dashed (black) curve with $\Gamma_g=0$, $\delta_3=0.01$], and both (dotted (pink) curve with $\Gamma_g=\delta_3=0.01$). All units are normalized to Γ_0.

quantum state and the resulting state projection slow down the naturally oscillatory evolution associated with coherent coupling. Repeated inspection goes unnoticed for the incoherent spin flip process, as the exponential decay associated with this process starts off linearly, whereas the coherent evolution starts off quadratically in time.

The divergence of the coherent spin jump in the weak-pumping limit is caused by a similar divergence in the lifetime of the ground-state coherence ρ_{13} under $\mathcal{L}_0$ evolution only. This divergence can be tentatively removed by incorporating the ground-state spin flip process at a rate Γ_g into the description. We do this by modifying the exponent in the integrand of Eq. (7) from $\exp(\mathcal{L}_0\tau)$ to $\exp(\mathcal{L}_0+\mathcal{L}_2)\tau$. This inclusion modifies Eq. (19) into the more physical form

$$R_{\mathrm{coh},+\to-} \approx \frac{\Omega_g^2}{2\Gamma_g'}, \tag{20}$$

where the total decay rate of the ground-state coherence

$$\Gamma_g' = \Gamma_g + \frac{\Omega_+^2+\Omega_-^2}{2\Gamma_0} \tag{21}$$

combines the natural incoherent spin flip rate Γ_g with an extra pump-induced decoherence rate $\Gamma_{\mathrm{extra}}=(\Omega_-^2+\Omega_+^2)/(2\Gamma_0)$. For three-level systems, a similar extension with part of the slow dynamics changes the general expressions for the jump rate in three-level systems derived by Nienhuis [32] into the more specific expressions discussed by Kimble *et al.* [21].

D. Jump rate at frequency detuning

Finally, we extend our four-level model to the general case by including the frequency detunings δ_2, δ_3, and δ_4 (see Fig. 1). These detunings are easily incorporated in the superoperator $\mathcal{L}_0$ and the associated steady-state distributions ρ_+ and ρ_- given by Eqs. (9)–(11). Substitution of the modified $\mathcal{L}_0$ and the original $\mathcal{L}_1$ and $\mathcal{L}_2$ in the generic Eq. (7) again yields expressions for the "coherent" jump rates R_{coh}. As the resulting expressions are too lengthy to display we will concentrate on the case of limited optical detuning ($\delta_2, \delta_4 \ll \Gamma_0$). We will, however, take the full evolution of the ground-state coherence into account, including both the spin flip rate Γ_g and a possible ground-state detuning $\delta_3 \neq 0$ in the evolution $\exp(\mathcal{L}_0+\mathcal{L}_2)\tau$. This results in an extension of Eq. (15) to

$$R_{\mathrm{coh},+\to-} = \mathrm{Re}\left(\frac{2\Gamma_0^5\Omega_g^2+\Gamma_0^3(\Omega_+^2+\Omega_-^2)\Omega_g^2+2\Gamma_0\Omega_+^2(\Omega_-\Omega_g+\Omega_+\Omega_e)^2}{(\Gamma_0^2+2\Omega_+^2)[2\Gamma_0^2(\Omega_+^2+\Omega_-^2+2\Gamma_0\{\Gamma_g+i\delta_3\})+(\Omega_+^2-\Omega_-^2)^2]}\right), \tag{22}$$

Note how the spin flip rate Γ_g and the ground-state detuning δ_3 have comparable effects; they both modify the built up of ground-state coherence that is the first step toward a coherently driven spin change. These effects are only visible at relatively weak-pumping ($\Omega_+^2+\Omega_-^2 < 2\Gamma_0\sqrt{\Gamma_g^2+\delta_3^2}$).

Figure 4 shows how the divergence in the calculated jump rate is removed both for a finite spin flip rate Γ_g and a finite ground-state detuning δ_3. The depicted curves are based on Eq. (22). In the weak-pumping limit, this equation predicts a limiting jump rate $R_{\mathrm{coh},+\to-} \approx \mathrm{Re}\{\Gamma_g^2/[2(\Gamma_g+i\delta_3)]\}$. For the frequency-degenerate system ($\delta_3=0$), this limit is $\Gamma_g^2/(2\Gamma_g)$; for the frequency-detuned system this limiting value is lower. At sufficiently large frequency detuning ($\delta_3 \gg \Gamma_g$) the jump rate even becomes practically zero in the weak-pumping limit, when none of the other interactions is strong enough to overcome the dominant frequency splitting δ_3.

V. EXPERIMENTAL POSSIBILITIES

Quantum jumps in the spin state should be observable as jumps in any spin-dependent observable, such as the measured Faraday [15] of Kerr effect [16], or the (polarization of the) spontaneous emission [4]. Most of these observables, however, provide only a weak measurement of the spin state. At a typical Faraday rotation angle of less than 1 mrad [15] more than 10^6 photons are needed to measure the spin state with sufficient certainty, making it practically impossible to observe the predicted quantum jumps by Faraday rotation.

We propose to search for spin quantum jumps by monitoring the corresponding changes in the reflectivity of an encompassing optical cavity. As this reflectivity can potentially change from 0 to 100% upon a spin flip [14], this measurement can be very efficient. It thereby presents a strong quantum measurement that projects the spin system onto an eigenstate. Changes in the cavity reflectivity from 0 to 50% due to the presence or absence of an optical transition have already been observed experimentally for a single InAs quantum dot in a high-finesse GaAs/AlGaAs cavity [7]. Similar systems should allow for an almost direct measurement of the spin state through the simple observation of the presence or absence of reflected photons of a specific polarization.

Whatever the inspection technique, one will generally try to extract the jump dynamics from a statistical analysis of the time dependence of the spin-sensitive inspection channels $I_+(t)$ and $I_-(t)$. For the proposed reflectivity measurement [7] these inspection channels are just the reflected intensities of the two circular polarizations. Typical quantities to measure are correlation functions such as

$$C_{\pm\pm}(\Delta t) \equiv \langle I_{\pm}(t) I_{\pm}(t+\Delta t)\rangle_t \tag{23}$$

where the brackets $\langle\ \rangle_t$ denote averaging over time. These correlation functions obey the same time evolution as the associated populations [23]; they generally decay exponentially at precisely the jump rates that we want to determine [34]. The modulation contrast of these correlation functions is linked to the criterium of strong versus weak measurements mentioned above.

We now give an outline of a refined model that includes that back action of the electron spin on the intracavity field and the nuclear spins. As a result of the backaction of the spin state on the intracavity optical field, this intracavity field will also perform jumps even if the injected field is constant. One approach to deal with this complication is to analyze the jump dynamics for two different but fixed states of the intracavity field, each one being associated with a different spin state of the quantum dot. If the cavity operates in the Purcell regime, the strong ac Stark shift will push the intracavity mode with the matched handedness out of resonance, thereby forcing the intracavity field to be circularly polarized in the handedness that has least interaction with the occupied spin state. This handedness is expected to switch abruptly (within the optical lifetime of the cavity) upon a quantum jump of the spin state. A second and more rigorous approach to include the backaction from the spin state on the intracavity field could be based on a rederivation of the state-selectivity reflectivity discussed in Ref. [14], but now for a four-level atomic system instead of the two-level system analyzed in that paper. This quantum-mechanical treatment would be a generalization of the so-called Maxwell-Bloch equations; it should result in an input-output formalism for the optical field operators in and outside a filled cavity [35]. For optical cavities with extremely large finesses, such that the cavity loss rate $\kappa \ll \Gamma_0$, other intriguing phenomena such as lasing of a single quantum dot have been predicted [36].

A second type of backaction involves the possibility of optical pumping of the nuclear spins through repetitive cycling in the spin-polarized optical transitions. This back action of the electron spins on the nuclear magnetic field has been observed experimentally in several studies [37,38]. The relevant time scale of this back action is much slower than that of the quantum jumps, as many electron cycles are needed before the nuclear magnetic field is seriously affected. Possible changes in the nuclear magnetic field can thus be included in a quasistatic way, where the field-related coupling parameters Ω_g, Ω_e, and δ_3 vary slowly in time. Whether such an approach is relevant and necessary will depend on future experiments.

VI. CONCLUDING DISCUSSION

We have presented a relatively simple model to describe the dynamics of a general four-level system. Using a separation of time scales between the fast spin-conserving optical transitions and slower spin-changing transitions, we predict the occurrence of sudden quantum jumps between spin-up and spin-down states under optical inspection. A natural interpretation of these jumps is as follows: the optical interaction first creates quantum entanglement between the atomic spin state and the optical polarization or emission direction of the interacting photon; a consecutive measurement on the photon will then project both the photon state and the spin state onto an eigenstate of the measurement operator. We distinguished between quantum jump due to incoherent spin flips and coherent spin coupling, derived expressions for both phenomena, and discussed the physical consequences. One example thereof is the quantum zero effect, where repetitive measurements and projection are predicted to reduce the jump rate associated with coherent spin coupling.

[1] A. Imamoglu, D. D. Awschalom, G. Burkard, D. P. DiVincenzo, D. Loss, M. Sherwin, and A. Small, Phys. Rev. Lett. **83**, 4204 (1999).
[2] A. J. Ramsay, S. J. Boyle, R. S. Kolodka, J. B. B. Oliveira, J. Skiba-Szymanska, H. Y. Liu, M. Hopkinson, A. M. Fox, and M. S. Skolnick, Phys. Rev. Lett. **100**, 197401 (2008).
[3] X. Xu, B. Sun, P. R. Berman, D. G. Steel, A. S. Bracker, D. Gammon, and L. J. Sham, Nat. Phys. **4**, 692 (2008).
[4] M. Paillard, X. Marie, P. Renucci, T. Amand, A. Jbeli, and J. M. Gérard, Phys. Rev. Lett. **86**, 1634 (2001).
[5] J. M. Taylor, J. R. Petta, A. C. Johnson, A. Yacoby, C. M. Marcus, and M. D. Lukin, Phys. Rev. B **76**, 035315 (2007).
[6] R. J. Warburton, C. Schäflein, D. Haft, F. Bickel, A. Lorke, K. Karrai, J. M. Garcia, W. Schoenfeld, and P. M. Petroff, Nature (London) **405**, 926 (2000).
[7] M. T. Rakher, N. G. Stoltz, L. A. Coldren, P. M. Petroff, and D. Bouwmeester, Phys. Rev. Lett. **102**, 097403 (2009).
[8] J. M. Gérard, B. Sermage, B. Gayral, B. Legrand, E. Costard,

and V. Thierry-Mieg, Phys. Rev. Lett. **81**, 1110 (1998).
[9] M. Bayer, F. Weidner, A. Larionov, A. McDonald, A. Forchel, and T. L. Reinecke, Phys. Rev. Lett. **86**, 3168 (2001).
[10] J. P. Reithmaier, G. Sek, A. Löffler, C. Hofmann, S. Kuhn, S. Reitzenstein, L. V. Keldysh, V. D. Kulakovskii, T. L. Reinekce, and A. Forchel, Nature (London) **432**, 197 (2004).
[11] T. Yoshie, A. Scherer, J. Hendrickson, G. Khitrova, H. M. Gibbs, G. Rupper, C. Ell, O. B. Shchekin, and D. G. Deppe, Nature (London) **432**, 200 (2004).
[12] D. Englund, D. Fattal, E. Waks, G. Solomon, B. Zhang, T. Nakaoka, Y. Arakawa, Y. Yamamoto, and J. Vučković, Phys. Rev. Lett. **95**, 013904 (2005).
[13] S. Strauf, N. G. Stoltz, M. T. Rakher, L. A. Coldren, P. M. Petroff, and D. Bouwmeester, Nat. Photonics **1**, 704 (2007).
[14] A. Auffèves-Garnier, C. Simon, J. M. Gérard, and J. P. Poizat, Phys. Rev. A **75**, 053823 (2007).
[15] M. Atatüre, A. Badolato, and A. Imamoglu, Nat. Phys. **3**, 101 (2007).
[16] J. Berezovsky, M. H. Mikkelsen, N. G. Stoltz, L. A. Coldren, and D. D. Awschalom, Science **320**, 349 (2008).
[17] H. G. Dehmelt, Bull. Am. Phys. Soc. **18**, 1521 (1973).
[18] R. J. Cook and H. J. Kimble, Phys. Rev. Lett. **54**, 1023 (1985).
[19] D. J. Wineland and W. M. Itano, Phys. Lett. **82A**, 75 (1981).
[20] J. C. Bergquist, R. G. Hulet, W. M. Itano, and D. J. Wineland, Phys. Rev. Lett. **57**, 1699 (1986).
[21] H. J. Kimble, R. J. Cook, and A. L. Wells, Phys. Rev. A **34**, 3190 (1986).
[22] K. T. Shimizu, R. G. Neuhauser, C. A. Leatherdale, S. A. Empedocles, W. K. Woo, and M. G. Bawendi, Phys. Rev. B **63**, 205316 (2001).
[23] M. B. Plenio and P. L. Knight, Rev. Mod. Phys. **70**, 101 (1998).
[24] V. Delgado and J. M. Gomez Llorente, Phys. Rev. A **68**, 022503 (2003).
[25] J. Fischer, M. Trif, W. A. Coish, and D. Loss, e-print arXiv:0903.0527.
[26] O. Gywat, H.-A. Engel, D. Loss, R. J. Epstein, F. M. Mendoza, and D. D. Awschalom, Phys. Rev. B **69**, 205303 (2004).
[27] R. Hanson, L. P. Kouwenhoven, J. R. Petta, S. Tarucha, and L. M. K. Vandersypen, Rev. Mod. Phys. **79**, 1217 (2007).
[28] B. Eble, C. Testelin, P. Desfonds, F. Bernardot, A. Balocchi, T. Amand, A. Miard, A. Lemaître, X. Marie, and M. Chamarro, Phys. Rev. Lett. **102**, 146601 (2009).
[29] A. Högele, B. Alén, F. Bickel, R. J. Warburton, P. M. Petroff, and K. Karrai, Physica E **21**, 175 (2004).
[30] M. Bayer, G. Ortner, A. Kuther, O. Stern, A. A. Gorbunov, A. Forchel, P. Hawrylak, S. Fafard, K. Hinzer, T. L. Reinecke, S. N. Walck, J. P. Reithmaier, F. Klopf, and F. Schäfer, Phys. Rev. B **65**, 195315 (2002).
[31] B. D. Gerardot, D. Brunner, P. A. Dalgarno, P. Ohberg, S. Seidl, M. Kroner, K. Karrai, N. G. Stoltz, P. M. Petroff, and R. J. Warburton, Nature (London) **451**, 441 (2008).
[32] G. Nienhuis, Phys. Rev. A **35**, 4639 (1987).
[33] G. J. Milburn, J. Opt. Soc. Am. B **5**, 1317 (1988).
[34] Th. Basché, W. E. Moerner, M. Orrit, and H. Talon, Phys. Rev. Lett. **69**, 1516 (1992).
[35] C. W. Gardiner and M. J. Collett, Phys. Rev. A **31**, 3761 (1985).
[36] O. Benson and Y. Yamamoto, Phys. Rev. A **59**, 4756 (1999).
[37] L. Childress, J. M. Gurudev, and A. S. Taylor, Science **314**, 281 (2006).
[38] A. I. Tartakovskii, T. Wright, A. Russell, V. I. Fal'ko, A. B. Van'kov, J. Skiba-Szymanska, I. Drouzas, R. S. Kolodka, M. S. Skolnick, P. W. Fry, A. Tahraoui, H. Y. Liu, and M. Hopkinson, Phys. Rev. Lett. **98**, 026806 (2007).